Journal of Molecular Structure 1156 (2018) 550–558

Contents lists available at ScienceDirect

Journal of Molecular Structure

journal homepage: http://www.elsevier.com/locate/molstruc

Structural insights into two inorganic-organic hybrids based on chiral amino acids and polyoxomolybdates

Mina Arefian, Masoud Mirzaei*, Hossein Eshtiagh-Hosseini

Department of Chemistry, Faculty of Science, Ferdowsi University of Mashhad, 917751436 Mashhad, Iran

ARTICLE INFO

Article history:
Available online 5 December 2017

Keywords:
Polyoxometalate
Inorganic-organic hybrid
Chirality
Histidine
Proline
Unconventional contacts

ABSTRACT

A new chiral inorganic-organic hybrid with the formula (L-His)$_2$($H_7CoMo_6O_{24}$)·$6H_2O$ (**1**), based on natural amino acid and Anderson type polyoxomolybdate was synthesized through mild condition. The chiral L-histidine molecules induced chirality to the whole structure through various types of strong and unconventional hydrogen bond (HB) interactions (CH···O, NH···O and CH···π interactions), as well as bifurcated hydrogen bonds (BHBs) between L-histidine amino acid, hexamer water cluster molecules, and $H_7CoMo_6O_{24}·xH_2O$. Following, important non-covalent CH···O interactions is investigated in another chiral inorganic-organic hybrid structure, (L-Pro)$_3$($PMo_{12}O_{40}$).$4.5H_2O$ (**2**), in detail. The CH···O hydrogen bonds lead to a chiral network similar to the DNA strands affording a promising candidate to bio-inorganic studies.

1. Introduction

Polyoxometalates (POMs), the versatile class of metal-oxygen also called isopolyanions/heteropolyanions, are extremely diverse family of anionic clusters with identified geometries [1], which are aggregates of oxo ligands and early transition metals in their highest oxidation state [2]. Introducing changes in their size, shape, composition, charge density, solubility, redox potential and acid strength, giving rise to a vast number of possible applications in different fields from catalysis to medicine [3]. In each of these application areas it would be desirable to have chiral POMs, since much biological activity is expected to depend on the chiral configuration, and chiral-selectivity in catalysis is also a major goal [4].

In recent years different groups interested in synthesis of prominent chiral POMs or chiral POM based materials [1,4–10].

However, it is not always simple to create chiral POM-based compounds, the instability and rapid racemization in solution make most POMs with chiral structures lose their chirality, so that racemic mixtures are usually found both in solution and in the crystalline state [11,12]. Fortunately, the ability to induce chirality by using chiral organic moieties or metal-organic frameworks points to a promising approach for fabricating new chiral inorganic-organic hybrids through various types of non-covalent interactions in crystal structure. One of the most powerful strategies to achieve synthetically chiral POM based materials is to functionalize POMs with biomolecules, especially enantiopure amino acids. Amino acids could induce their valuable properties, such as chirality and biochemical characteristics to the whole inorganic-organic hybrid structure. Moreover, they are water-soluble, commercially available, nontoxic compounds, and have an intimate relationship to the organism's life activities for studying in medical applications. The presence of several groups capable of forming different types of H-bonds on amino acids side chains lead to POM-AA hybrids with a variety of architectures and topologies. The strong and weak H-bonds are the most important factor in occurring particular biological structures such as DNA and protein molecules.

The circular dichroism (CD) spectroscopy is a very beneficial and common method to investigate the chirality of compounds [13,14], but it provides no specific structural information at the atomic level. The interference of any compound which absorbs in desired wavelength makes this approach restricted, unless it can be proved that the compound in question, will not mask the target compound signal [15]. Absolute configurations of a chiral molecule (in pure form) are most often obtained by X-ray crystallography precisely. In X-ray crystallography, the Flack parameter is a factor used to

* Corresponding author.
E-mail address: mirzaeesh@um.ac.ir (M. Mirzaei).

https://doi.org/10.1016/j.molstruc.2017.12.001
0022-2860/

determine the chirality in a spatial arrangement of atoms in solid state which consider the absolute structure of a non-centrosymmetric crystal, so it is a powerful approach to detect chirality and also study the desired compound in atomic level and responsible interactions to create such a chiral structure precisely [16].

To date, the inorganic–organic entities based on the well-known POMs, such as Keggin, Wells-Dawson and Lindquist type, have been successfully reported. In contrast, the use of Anderson-type polyoxoanions as inorganic building blocks in this aspect remains largely unexplored [17].

The highly water soluble Anderson–Evans POM has a very special structure with the average dimensions 8.6 × 8.6 × 2.7 $Å^3$ which allows positioning of this POM into narrow protein clefts or migration through narrow channels inaccessible for larger POMs, and make it suitable choice for protein crystallization. To our knowledge, only little structure information is available regarding the L-His–POM in Cambridge Structure Database (CSD) [18]. Thus, compound **1** provides an opportunity to probe the interaction of L-histidine (L-His) amino acid as protein building blocks, and Anderson type POM in detail.

Histidine contains a side chain imidazole, classifying it as amino acid with polar side chain which is capable of being positively charged at physiological pH. While usually hydrophobic amino acid residues such as proline occupy the core, polar and charged amino acids preferentially cover the surface of the protein molecules and are in contact with environment and solvent due to their ability to form hydrogen bonds. At this point of view, we focused our attention to L-His interaction with POM and water clusters in **1**, where our main attention focused toward Proline (Pro) interactions to each other in crystal structure of **2**.

Pro presents in chiral compound **2** are the only natural amino acid with an aliphatic ring that comprises both the “main” and the “side-chain” in proteins. It is also unique because, once it forms a peptide bond; it no longer possesses covalently bonded hydrogen. Therefor it is not expected to occur in a α-helix or in a β-strand of proteins. Nevertheless, Pro is found in the middle of α-helices. This has been explained by the existence of a unconventional C–H···O hydrogen bond involving the ring C–H groups. It is interesting that the above mentioned characteristic, normally found in naturally occurring systems, has been observed in an “artificial” (synthesized) compound.

To further explore the interaction between heteropolymolybdates with L-histidine and proline, we synthesized $(C_6H_9N_3O_2)_2(H_7CoMo_6O_{24})\cdot 6H_2O$ **1** and investigated the structure of this hybrid POM in comparison with $[C_5H_{10}NO_2]_3[P\text{-}Mo_{12}O_{40}].4.5H_2O$ **2.** These hybrid POMs, contain combination of electrostatic forces and hydrogen bonding, rendering them stable in the solid and solution states and result in the first chiral Anderson-type POM based hybrid with L-histidine.

2. Experimental

2.1. Material and methods

All reagents were purchased commercially and used without further purification. The FTIR spectra were recorded in the range 4000–400 cm^{-1} with an Avatar 370 Thermo Nicolet spectrometer using KBr pellets. The C, H, and N elemental analyses were performed with a Thermo Finnigan Flash model 1112 EA micro-analyzer. The Mo and Co contents ratio were measured by atomic absorption spectroscopy.

2.2. Chemical preparation

To prepare polyoxometalate, the previously developed method was used [19], resulting in $(NH_4)_6[Co_2Mo_{10}O_{38}H_4]\cdot 7H_2O$ (here in Co2Mo10), product. 3.75 g (3.05 mmol) of $(NH_4)_6Mo_7O_{24}$ $4H_2O$ dissolved in about 20 mL of water by stirring, then 0.775 g (3.10 mmol) of $Co(CH_3COO)_2{}^{\prime}4H_2O$ dissolved in about 15 mL of water was added dropwise. A total of 0.8 g active charcoal and 5 mL of peroxide solution (18%) was added, which induces a color change from pink to black. After boiling the black solution for 1 h, the active charcoal is separated by filtration.

Dark green crystals of as prepared Co_2Mo_{10} (80 mg, 0.042 mmol) dissolved in 5 ml water. Then a solution of L-His (40 mg, 0.25 mmol) in 5 ml water and 0.5 ml HCl 2 M, added dropwise to the first solution while stirring in 70 °C. The pH of reaction adjusted around 3.5 along half an hour. After stirring the reaction solution for 2 h, it was filtered and the filtrate was kept for 2 months at room temperature and then green needle-shaped crystals suitable for single crystal X-ray diffraction were collected. Anal. Calc. for C_{12} H_{34} Co Mo_6 N_6 O_{34}: C, 9.99; H, 2.36; N, 5.83; Co, 4.09, Mo, 39.98%. Found: C, 10.28; H, 2.54; N, 5.87; Co, 4.34; Mo, 39.11%, IR (KBr pellet, cm^{-1}) ν: 3134(bs), 1620(s), 1504(s), 1490(w), 1410(s), 1354(m), 1224(m), 1091(s), 923(s), 904(sh), 810(m), 701(m), 619(w).

Co_2Mo_{10} is a very sensitive precursor to solution pH, (stable between: 2.5–4) and slight changes in local pH of solution during reaction might change the product to its analogous. Although pH value controlled within the reaction, instability during long period of crystallization may cause transformation to Anderson $(H_6CoMo_6O_{24}\cdot xH_2O)$ type POM observed in this work.

2.3. X-ray crystallography

The corresponding experimental parameters of single crystal X-ray analysis of the title hybrids are given in Table 1. X-ray data for compounds were collected on Rigaku MicroMax-007HF diffractometer with Confocal Max Flux optic-monochromated Mo Kα radiation (λ = 0.71073 Å) and PILATUS 200 K detector. Crystallographic data were collected at a temperature of 150(2) K using CrystalClear-SM Expert 2.1 b29. The structure was solved by direct methods (SHELXT) and full-matrix, least-squares refinement of the structure was carried out with SHELXL-2014. Fig. 1.

3. Results and discussion

3.1. Structure description

An enantiomerically pure compound of classical Anderson-type polyoxoanion and L-His amino acid has been separated as green needle-shaped crystals from aqueous solution. Single-crystal X-ray analysis of **1** reveals that this compound consists of one Anderson type polyoxomolybdates $[HCo(OH)_6Mo_6O_{18}]^{2-}$ (abbreviated as $CoMo_6$) anion, two L-Histidinium, (abbreviated as L-His), and six different water molecules in asymmetric unit crystallized in *P*1 space group. All enantiomerically pure chiral molecules crystallize in one of the 65 Sohncke groups (chiral space groups). The Flack parameter was used to estimate the absolute configuration of a structural model determined by single-crystal structure analysis. If the value is near 0, with a small standard uncertainty, the correct structure might be the absolute structure given by the structure refinement while if the value is near 1, the possible structure will be the inverted one. If the value is near 0.5, the crystal could be racemic or twinned [16]. Here, the Flack parameter of **1** is −0.004, indicating that compound **1** is an optically pure hybrid compound.

The presences of protonated L-His molecules resemble the

Table 1
Crystal data and structure refinement for compound 1.

Empirical formula	C_{12} H_{34} Co Mo_6 N_6 O_{34}	
Formula weight	1441.02	
Temperature	100(2) K	
Crystal system	Triclinic	
Space group	P1	
Unit cell dimensions (Å), (°)	a = 9.1248(4)	α = 95.626(15)
	b = 10.7803(6)	β = 112.163(11)
	c = 11.7338(6)	ɤ = 114.997(10)
Volume (Å3)	922.12(12)	
Z	1	
Density (calculated)	2.595 Mg/m3	
Absorption coefficient	2.537 mm-1	
F(000)	699	
Crystal size	0.20 × 0.20 × 0.20 mm3	
Theta range for data collection	2.455–27.497°.	
Index ranges	−11 ≤ h<=11,-13 ≤ k<=13,-15 ≤ l<=15	
Reflections collected	20461	
Independent reflections	8112[R(int) = 0.0230]	
Completeness to theta = 27.497°	99.6%	
Absorption correction	Multi-scan	
Max. and min. transmission	0.786 and 0.605	
Refinement method	Full-matrix least-squares on F2	
Data/restraints/parameters	8112/28/544	
Goodness-of-fit on F2	1.022	
Final R indices [I > 2sigma(I)]	R1 = 0.0186, w$R2$ = 0.0486	
R indices (all data)	R1 = 0.0191, w$R2$ = 0.0487	
Flack parameter	x = −0.004(17)	
Largest diff. peak and hole	0.665 and −0.569 e.Å-3	

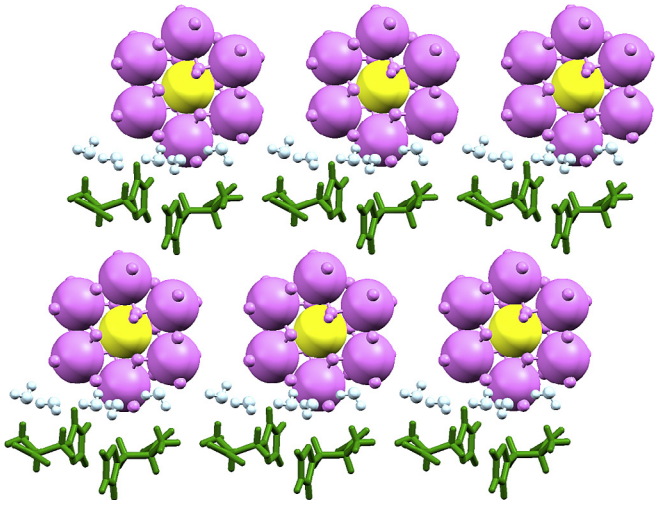

Fig. 1. Graphical abstract, Chiral Inorganic-organic Hybrid Garden (yellow and purple: POM, green: L-histidine, blue: water). (For interpretation of the references to colour in this figure legend, the reader is referred to the web version of this article.)

interactions occurring in the biological functions. A perspective view of compound **1** with its numbering scheme is shown in Fig. 2. In the title compound, $H_7CoMo_6O_{24}\cdot xH_2O$ with seven protons located calculatedly [20,21], comprises from octahedral unit CoO_6, surrounded by six MoO_6 groups. The six Mo atoms construct a hexagon around Co creating an overall disc shape anion. In these anions, there are three types of Mo–O bonds. The Mo atoms bonded to two terminal oxygen atoms with Mo–O_t distances in the range of 1.693(5)–1.726(4) Å. The Mo–O_b bonds ranging from 1.874(5) to 2.059(4) Å correspond to bridging oxygen atoms bonded to two molybdenum atoms. The longest Mo–O_c distances, 2.228(5)–2.312(3) Å belong to oxygen atoms coordinated to cobalt and molybdenum. The Co–Mo distances are in range of 1.901(4) to 1.936(5) Å which is in the common range for this type of bond [22].

Histidine contains an α-amino group (which is in the protonated $-NH_3^+$ form under biological conditions), a carboxylic acid group (which is in the deprotonated $-COO^-$ form under biological conditions), and a side chain imidazole, presence of these multiple active sites provide various possibilities to establish an extended network based on strong and also unconventional H-bond interactions.

Two symmetrically different L-His molecules (His-A showed in yellow color and His-B in purple) locate between two POM anions. This arrangement leads to pure inorganic ($CoMo_6$) and organic (His-A and His-B) chains alternatively (Fig. 3a).

There are N3A–H3A1···O1W interactions between His-A amino group and the first water molecule of six membered cluster as well as the weaker C5A-H5A···O13 (2.383 Å) interactions between $^{\alpha}$CH of His-A and terminal oxygen of $CoMo_6$ moiety resulting in POM linkage *via* amino acid units. In contrast, the second His-B (purple colored) is connected to both adjacent $CoMo_6$ units directly through imidazole ring segment interaction: N2B–H2B1···O14 and C2B–H2B···O12 to terminal and bridging oxygen atoms, respectively. Moreover C4B–H4B1···O23 and N3B–H3B3···O23 interactions linked His-B to the other adjacent $CoMo_6$ unit. Those directional interactions with different orientations lead to arrangement of His-A and B opposite to each other which eliminate any symmetry elements and distribute the chiral feature of L-His to the whole network. These interactions result in one-dimensional chains (Fig. 3a), connecting to each other and construct 2-D plane of alternative inorganic-organic chains (Fig. 3b). Mainly there are two categories of interactions between amino acids. First, direct interaction between a pair of A and B L-His species present in the same 1-D chain: C4A-H4A2···C_gB (2.615 Å, 151.04°) and C4B–H4B1···C_gA (2.869 Å, 110.74°) (Fig. 5). Second, C–H···π interactions considered as unconventional hydrogen bonds, which is characterized by C–H bond points to aromatic ring center with distance in the range of 2.6–3.0 Å [23]. It is worth mentioning that in biomolecules like proteins, cation···π interactions between L-His molecule and other organic moieties such as Phe, Tyr and Trp amino acids are frequently

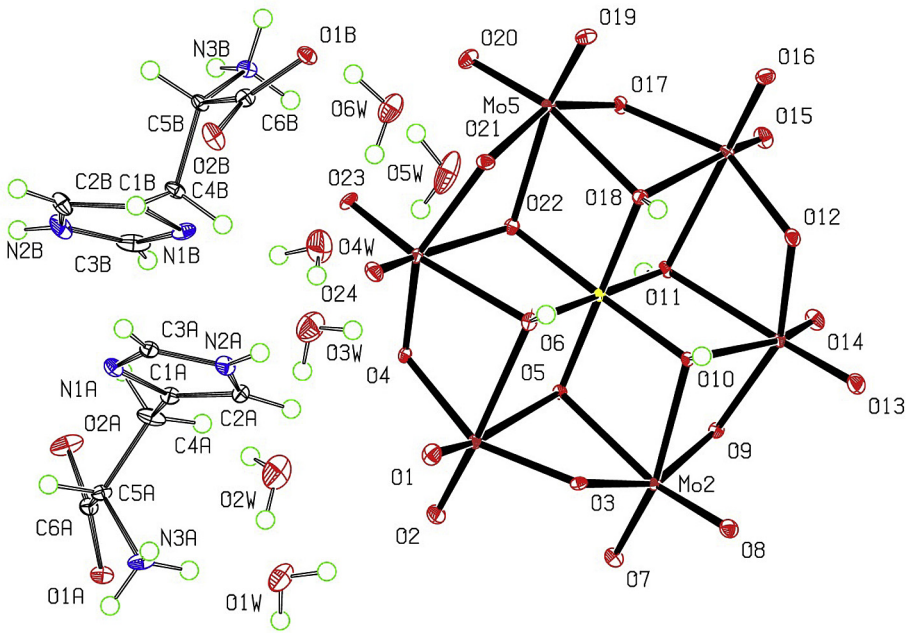

Fig. 2. A projection of the structure of compound 1, showing the displacement ellipsoid.

observed [24]. It is suggested that in compound **1**, the involvement of amine and carboxylate groups of L-His molecules in strong H-bonds with $CoMo_6$ moiety changes this tendency and causes the opposite direction of His-A and His-B toward each other, creating CH···π interactions between aliphatic CH_2 group of one L-His and imidazole ring of the other one. It would be attractive to design desirable interactions of POM and amino acids like histidine to provide inorganic drugs such as anti-amyloid agents for Alzheimer's disease [25]. The second category refer to each pair of His-A/His-B molecules linked to the rest of AA chain *via* N3AH3A2···O1B (2.057 Å) and N3BH3B1···O1A (2.005 Å) interactions (see Table 2). Moreover the lattice water molecules further reinforce the whole structure as they are able to play space-filling role where there are cavities of a suitable size [26]. Herein, there are six different water molecules (hereafter O1w to O6w) which create water channels between 2-D layers and a -3-D supramolecular network of $CoMo_6$-His (Fig. 6). Each water molecule of this six membered water cluster interacts differently to the POM and AA (Fig. 4). All H_2O molecules join to the three types of surface oxygen atoms of $CoMo_6$. *via* OH···O interactions Except O6W atom which interacts with H atom of $CoMo_6$ (O6H6···O6W). The interactions correspond to each member of water cluster reported in Table 3. As shown in Fig. 4, several three-centered hydrogen bonds were observed. Three-centered HBs (over-coordinated oxygen (OCO) and bifurcated hydrogen bonds (BHB)) have been used to explain a large number of interactions in biological systems and frequently occur in the crystal structures of zwitterionic amino acids (~70%) [27]. Although, it is demonstrated that OCO atoms occur much more frequently than BHBs [28], however, surprisingly, the bifurcated bonds (BHB) were observed in compound **1**.

It was proposed that in three-centered hydrogen bonds, the sum of the three angles formed by the H atom and those three atoms should be near to 360° (Scheme 1) [29]. The measurements of these angles confirm that these four atoms are almost located in a plan (Table 4) (see Fig. 7).

To exhibit the importance of unconventional CH···O interactions, compound **2** was investigated which contains $[PMo_{12}O_{40}]^{3-}$ units linked together by three prolinium in chiral $P2_1$ with 0.01 value for its Flack parameter [8]. The three "types" of Pro were labeled as A, B and C structures.

It can be seen that C and B Pros are directly connected to each other by weak hydrogen bonding [$O_{(1C)}\cdots O_{(1B)}$ 2.919 (4) Å] and do not have any interactions with A-Pro. Furthermore, the water molecules link these amino acids *via* their $O_{(2S)}$ atom through strong hydrogen bonding (Fig. 8). An interesting feature is the similarity of this crystal structure with that of proteins and peptides. The triple attachment of Pros with each other in the overall network occurs (we neglect the POMs here) by C–H···O bonds. The importance of C–H···O interactions, as a stabilizing feature in crystal structures, were recognized almost four decades ago [30]. These C–H···O interactions along the z-axis shown in Fig. 9, cause Pros to take up the spatial lattice positions similar to DNA (zigzag chains). In proteins, there are many C–H···O interactions of $^{\alpha}$C-H and $^{\gamma}$C-H that play an important role in the formation of the protein structures. The Pros in compound **2** have several interactions which might be classified according to the distances of the proline carbon and the nearest "hydrogen bonded" oxygen of the neighboring species (Table 5). These data indicate that the B-Pro in compound **2** acts in the same way as does proline in proteins. In both cases proline is engaged in "hydrogen bonding" interaction with $^{\alpha}$C-H and $^{\gamma}$C-H. This evidence could be attributed to the interaction of NH_3^+ and one of the terminal oxygens (O_t) of the POM, rendering carbon-bonded hydrogens somewhat acidic. Also, it is clear that $^{\alpha}$C-H and $^{\gamma}$C-H in A and C-Pros produce stronger hydrogen bonding interaction as compared to the other carbon atoms. Furthermore, our results indicate that A and C-Pro have C–H···O interaction with the POM present in the unit cell. As demonstrated by Fig. 10, these interactions occur between the $^{\alpha}$C-H of the A-Pro and the O_c of the POM, as well as between the $^{\delta}$C-H of the C-Pro and the O_b and O_t of the POM. However, the B-Pro is different due to the strong interaction between NH_3^+ and O_t of the POM.

The alternating positions of the B-Pros, on the two sides of the

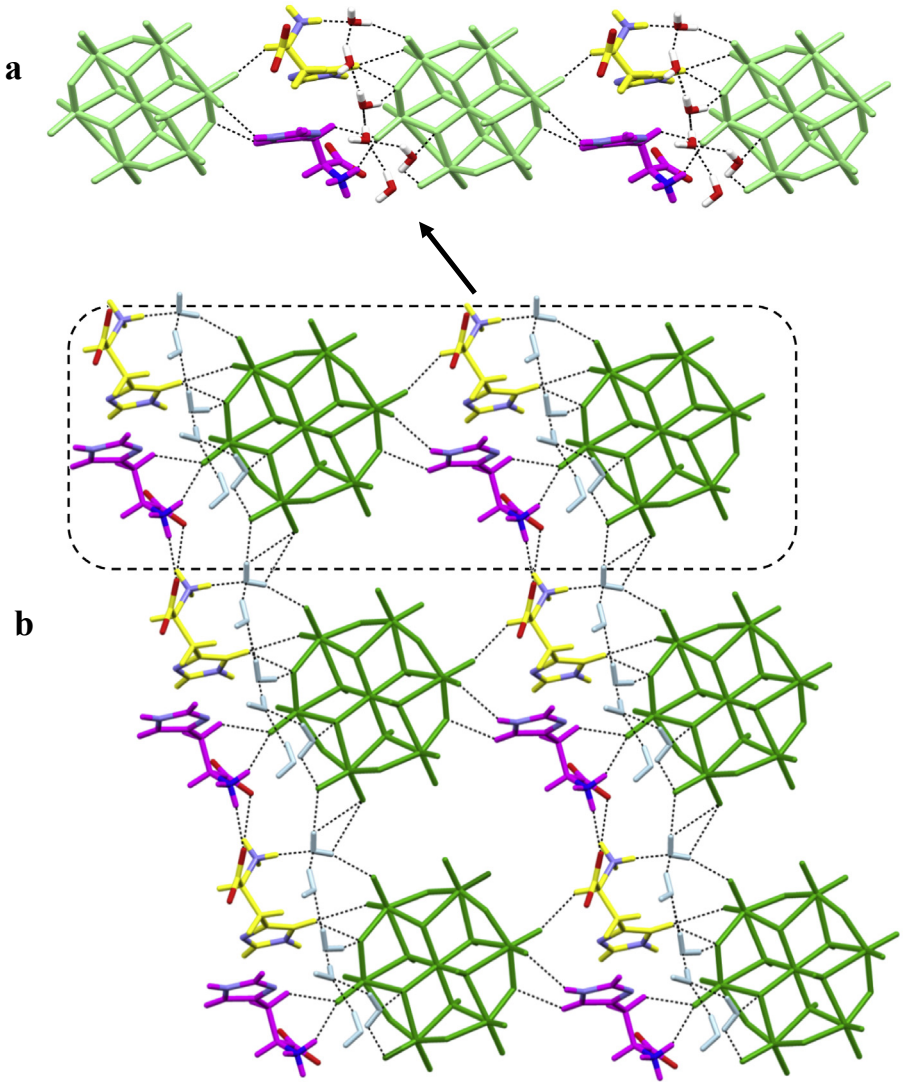

Fig. 3. 1-D CoMo6 and His-A/B chain 1a, and 2-D plane formed through 1-D chains linking.

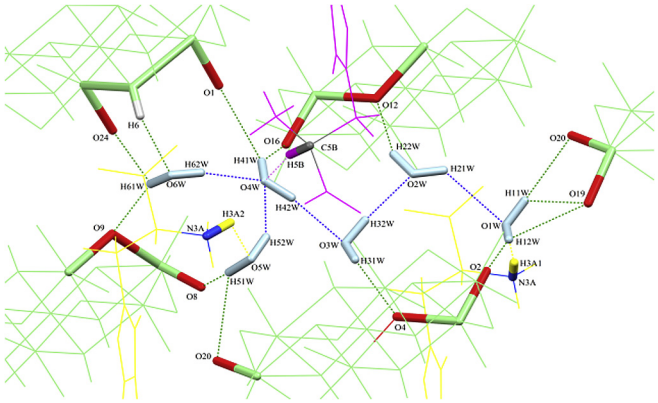

Fig. 4. Interaction environment around each of six different type water cluster molecules.

symmetry plane, play an essential role in the stability of the crystal structure (Fig. 11). There is some degree of non-covalent overlap between neighboring POMs (with a distance of 2.814 (4) Å between their terminal oxygen atoms) which might be partly brought about by the protonated amine group of the B-Pro (Fig. 12). This type of spacing is not observed between two pure POM acids. Therefore, one might conclude that amino acids in general and proline in particular, may have a stabilizing effect on the lattice.

3.2. Infrared spectroscopy

Vibrational spectrum of compound **1** exhibits the characteristic bands associated with the building constituent: three characteristic bands in 1700-1400, 1000-800 and 600-800 cm^{-1}, attributed to OH and NH bending frequencies, Mo–O terminal stretching, Mo–O bridging stretching, respectively which are in good agreement with similar structures. The bands observed in lower intensities are difficult to assign due to vibration of Co–O bonds and water liberation [31]. As it is expected the intensity of characteristic frequencies of 941–909 cm^{-1} correspond to symmetric stretching vibration of Mo=O (terminal) reduced, due to involvement of terminal oxygen atoms in H-bonds with amino acid and water molecules. The stretching vibrations of Mo=O (terminal) bond is shifted towards lower wave numbers compared to those of pure POM. On the other hand, the bands around 1500-1000 cm^{-1} region

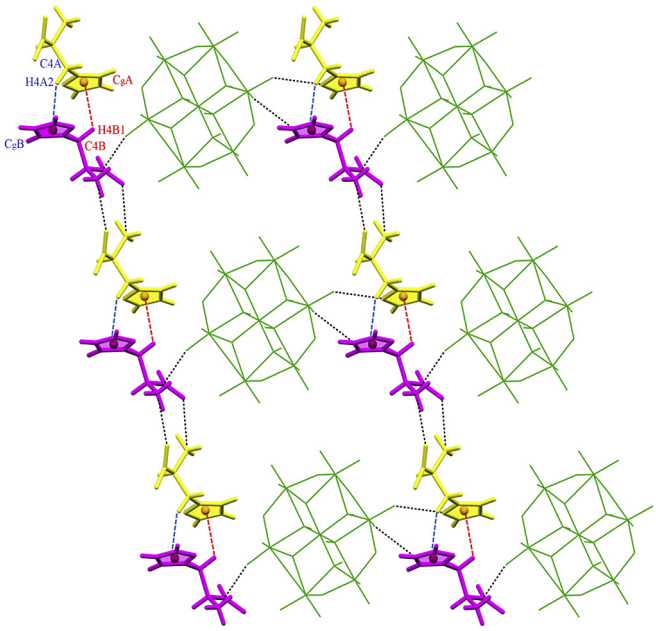

Fig. 5. Partial view of the crystal packing of compound 1 with indication of the intermolecular CH ··· π interaction established between the His-A and His-B imidazole rings.

Table 2
Hydrogen bonds between His-A/B and CoMo6 unit geometry (Å, °).

D-H···A	D-H	H···A	D···A	D-H···A
N3AH3A1···O1W	0.899	1.924	2.823	168.67
C5AH5A···O13	0.875	2.383	3.258	145.66
C2AH2A···O1	0.833	2.534	3.367	146.41
C2AH2A···O4	0.785	2.675	3.460	140.28
N2BH2B1···O14	0.822	2.569	2.991	110.39
C2BH2B···O12	0.812	2.561	3.373	143.54
C4BH4B1···O23	0.639	2.501	3.140	121.99
N3BH3B3···O23	0.852	1.953	2.805	155.02

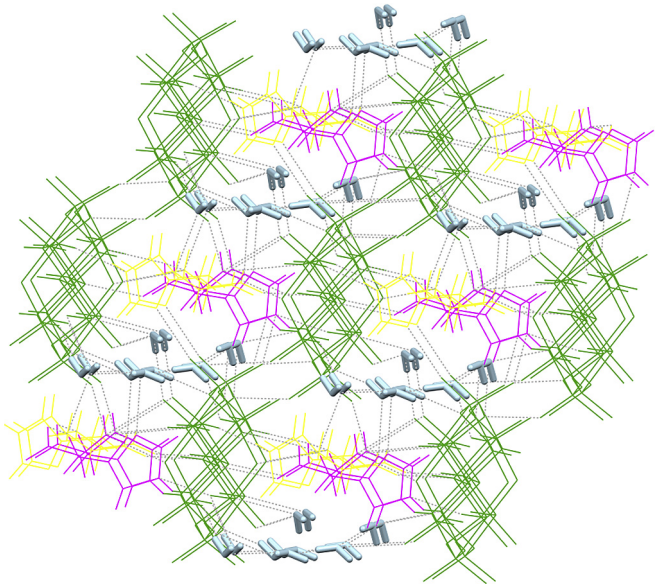

Fig. 6. A view of the 3-D supramolecular structure in **1**.

Table 3
Hydrogen-bond geometry (Å, °) for each H_2O molecule of six membered water cluster with adjacent species: H_2O, POM and amino acid separately. Bifurcated hydrogen bond atoms represented underlined.

Adjacent species	D-H···A	D-H	H···A	D···A	D-H···A
H_2O (1)					
H_2O	O2WH21W···O1W	0.847	2.272	3.119	127.22
POM	O1WH11W···O20	0.852	2.229	3.081	175.60
	O1WH11W···O19	0.850	2.622	3.474	110.10
	O1WH12W···O19		2.651	3.501	107.96
	O1WH12W···O2		2.126	2.976	158.47
AA	N3AH3A1···O1W	0.910	1.924	2.834	168.67
H_2O (2)					
H_2O	OW3H32W···O2W	0.851	1.890	2.741	173.15
POM	O2WH22W···O12	0.848	1.961	2.809	155.95
AA	–	–	–	–	–
H_2O (3)					
H_2O	O4WH42W···O3W	0.854	1.944	2.798	171.33
POM	O3WH31W···O4	0.850	2.094	2.944	148.08
AA	–	–	–	–	–
H_2O (4)					
H_2O	O5WH52W···O4W	0.85(2)	2.280	3.13	149.73
	O6W H62W···O4W	0.850	2.007	2.857	165.10
POM	O4WH41W···O16	0.852	2.270	3.122	145.89
	O4WH41W···O1		2.453	3.305	120.20
AA	C5BH5B···O4W	1.000	2.212	3.212	166.07
H_2O (5)					
H_2O	–	–	–	–	–
POM	O5WH51W···O20	0.85(6)	2.633	3.483	108.71
	O5WH51W···O8		2.146	2.996	149.54
AA	N3A H3A2···O5W	0.910	2.542	3.452	121.17
H_2O (6)					
H_2O	–	–	–	–	–
POM	O6H6···O6W	0.850	1.887	2.737	151.95
	O6WH61W···O24	0.851	2.669	3.52	127.17
	O6WH61W···O9		2.085	2.936	154.30
AA	–	–	–	–	–

are assignable to imidazole ring, C—N and C—OH bonds, in which the band in 1091 cm^{-1} assigned to ν(C—N) and 1504 cm^{-1} associated to ν(C=N) are the characteristic ones [32] and confirm the presence of amino acid and POM in the compound. The bands exhibited in IR spectrum of Co_2Mo_{10} and $CoMo_6$ are almost very similar to each other, so it is not possible to distinguish them accurately [31]. Finally, a broad band around 3000-3500 cm^{-1} is attributed to the ν(OH) vibration of coordinated and water cluster molecules. The broadness of this band indicates clearly the strong hydrogen-bonding interactions in the crystal structure. In summary, these results are in good agreement with X-ray crystallography results.

4. Conclusion

In this study, we reported the synthesis of novel chiral material based on L-histidine amino acid and Anderson type polyoxomolybdate. Since chiral POM based compounds rarely reported and also their applications are very interesting especially in bio-inorganic fields, we were involved in surveying all noncovalent interactions ranging from strong H-bonds (NH···O and OH···O) to unconventional ones such as CH···π and CH···O as well as bifurcated H-bonds in water clusters in two hybrids of polyoxomolybdate and natural amino acids (L-His, L-Pro). Chiral POM-based hybrid materials having both functionality of chiral materials and POMs, seized considerable attentions due to extended applicable potential in medicine and enantioselective catalysis. Further we tried to find relationships between structural behavior of these compounds and natural behavior of amino acid, protein and DNA in order to shed more light in bio-inorganic chemistry.

Table 4
Three angles around each of bifurcated H atoms of water cluster molecules (°).

Bifurcated H atom	Angle I		Angle II		Angle III		Sum of three angles
H11W	O1H11W···O20	175.60	O1H11W···O19	110.10	O20···H11W···O19	67.23	352.93
H12W	O1H12W···O19	107.95	O1H12W···O2	158.47	O19···H12W···O2	88.88	355.3
H41W	O4H41W···O1	120.20	O4H41W···O16	145.8	O1···H41W···O16	93.35	359.35
H61W	O6H61W···O9	154.30	O6H61W···O24	127.17	O24···H61W···O9	77.83	359.3
H51W	O5H51W···O20	108.71	O5H51W···O8	149.54	O8···H51W···O20	92.97	351.22

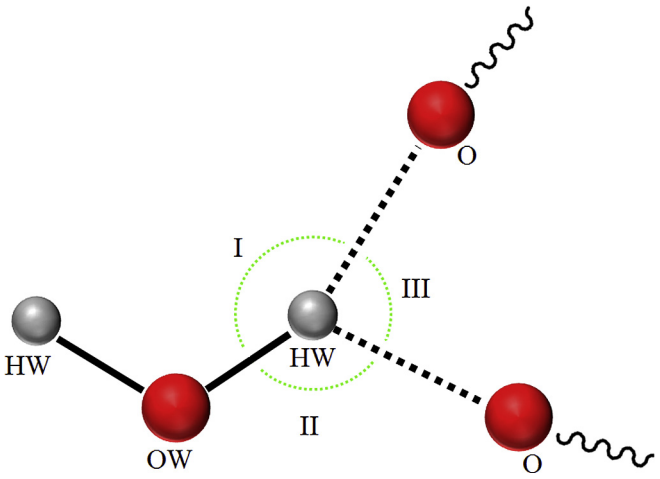

Fig. 7. Schematic view of BHB illustrating three measured angles (W indicate the H and O atoms relating to water molecule).

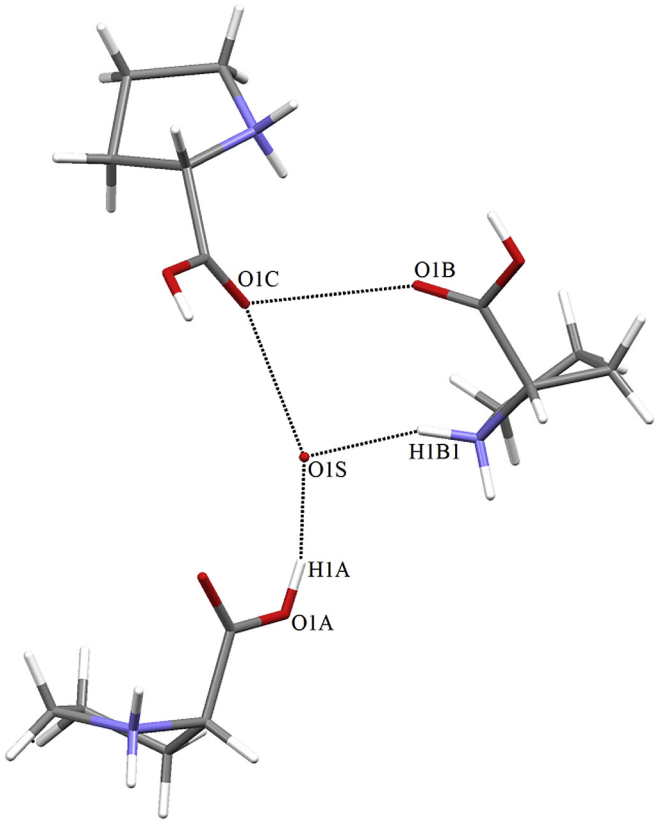

Fig. 8. Representation of observed C–H···O interactions between proline molecules along z-axis.

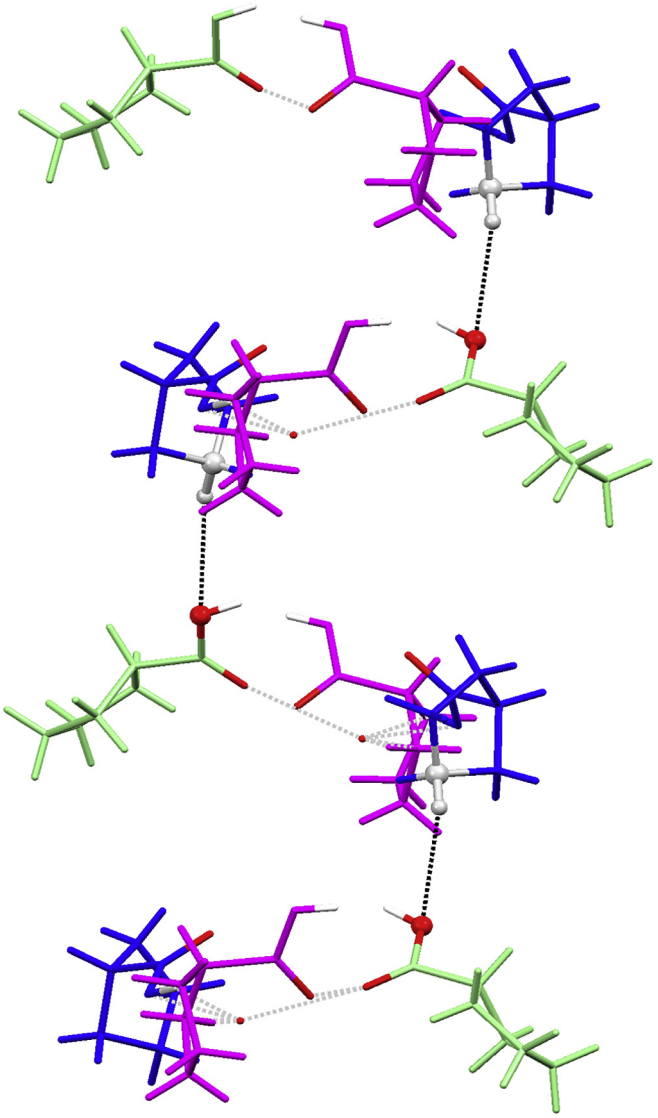

Fig. 9. Representation of observed C–H···O interactions between proline molecules along z-axis, showed with black dashed line, (A-Pro: blue, B-Pro: purple and C-Pro: light green). (For interpretation of the references to colour in this figure legend, the reader is referred to the web version of this article.)

Table 5
Average distance (Å) and number of C–H···O interactions for each proline and C–H bond in compound 2.

Interactions	C^{α}-H···O	C^{β}-H···O	C^{γ}-H···O	C^{δ}-H···O
Pro-A	2.502/2	2.696/2	2.558/2	0
Pro-B	2.692/3	0	2.704/3	2.719/2
Pro-C	2.635/2	2.703/1	2.526/3	2.686/1

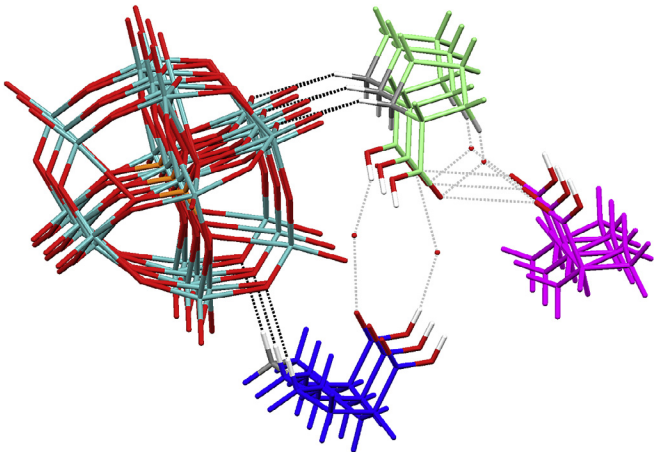

Fig. 10. The $^{\alpha}$C-H and $^{\delta}$C-H interactions of the A and C Pros with different oxygen atoms of the POM showed with black dashed line, (A-Pro: blue, B-Pro: purple and C-Pro: light green). (For interpretation of the references to colour in this figure legend, the reader is referred to the web version of this article.)

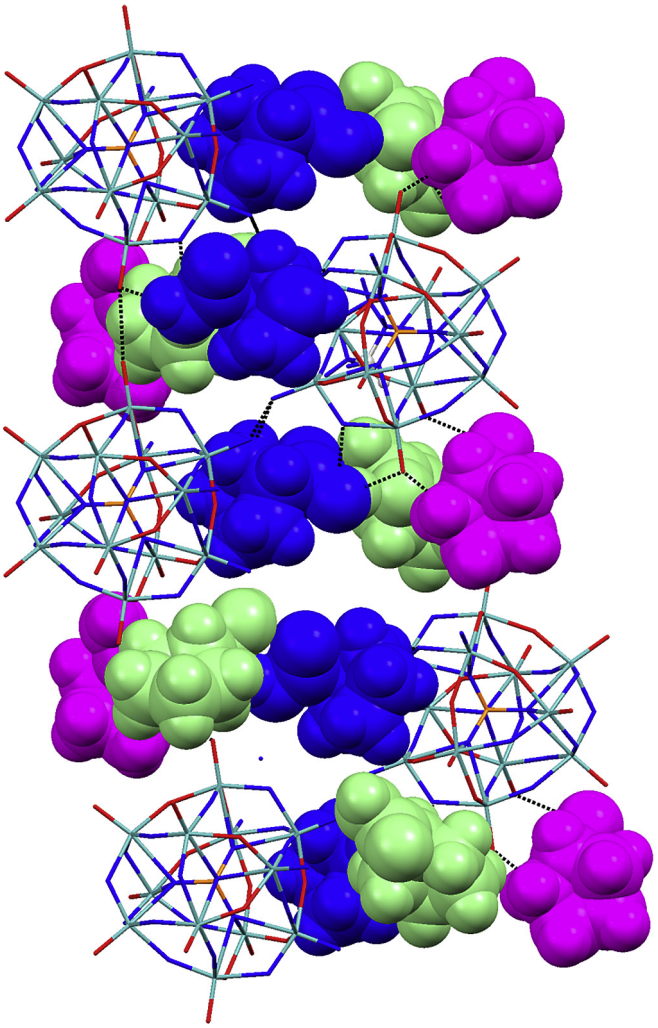

Fig. 11. The effect of alternating position of the B-Pro in the stabilization of crystal structure, (A-Pro: blue, B-Pro: purple and C-Pro: light green). (For interpretation of the references to colour in this figure legend, the reader is referred to the web version of this article.)

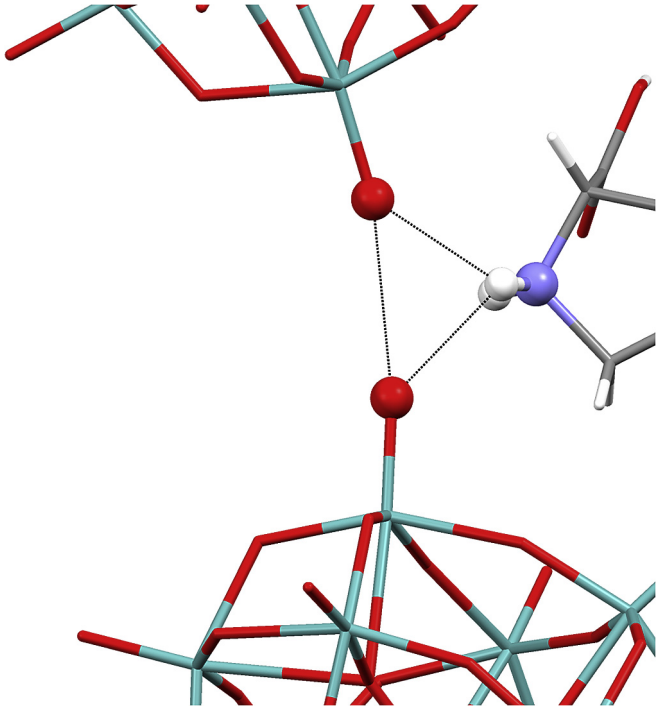

Fig. 12. Noncovalent overlap between neighboring POMs and amine group of B-Pro.

Acknowledgment

The Ferdowsi University of Mashhad is gratefully acknowledged for financial support of the work presented in this article (project no. 3/29636).

Supplementary data

Crystallographic data for the structures reported in this paper have been deposited with the Cambridge Crystallographic Data Center as supplementary publication no. CCDC-280411 [8] and 1552988. Copies of the data can be obtained free of charge an application to the CDCC, 12 Union Road, Cambridge CB2 1EZ, UK (e-mail: deposit@ccdc.cam.ac.uk).

References

[1] B. Hasenknopf, K. Micoine, E. Lacôte, S. Thorimbert, M. Malacria, R. Thouvenot, Chirality in polyoxometalate chemistry, Eur. J. Inorg. Chem. (2008) 5001–5013, https://doi.org/10.1002/ejic.200800759.
[2] M.T. Pope, Heteropoly and Isopoly Oxometalates, 1983, https://doi.org/10.1002/ange.19840960939.
[3] A. Proust, B. Matt, R. Villanneau, G. Guillemot, P. Gouzerh, G. Izzet, Functionalization and post-functionalization: A step towards polyoxometalate-based materials, Chem. Soc. Rev. 41 (2012) 7605–7622, https://doi.org/10.1039/c2cs35119f.
[4] F. Xin, M.T. Pope, Lone-pair-induced chirality in polyoxotungstate structures: tin(II) derivatives of a-type $XW_9O_{34}^{n-}$ (x = P, Si). Interaction with amino acids, J. Am. Chem. Soc. 118 (1996) 7731–7736, https://doi.org/10.1021/ja954045p.
[5] C. Boglio, B. Hasenknopf, G. Lenoble, P. Rémy, P. Gouzerh, S. Thorimbert, E. Lacôte, M. Malacria, R. Thouvenot, Sensing the chirality of dawson lanthanide polyoxometalates $[\alpha_1\text{-}LnP_2W_{17}O_{61}]^{7-}$ by multinuclear NMR spectroscopy, Chem. A Eur. J. 14 (2008) 1532–1540, https://doi.org/10.1002/chem.200701429.
[6] J. Zhang, Z. Zhao, J. Zhang, S. She, Y. Huang, Y. Wei, Spontaneous resolution of polyoxometalate-based inorganic–organic hybrids driven by solvent and common ion, Dalton Trans. 43 (2014) 17296–17302, https://doi.org/10.1039/C4DT01954G.
[7] J. Zhang, J. Luo, P. Wang, B. Ding, Y. Huang, Z. Zhao, J. Zhang, Y. Wei, Step-by-step strategy from achiral precursors to polyoxometalates-based chiral organic-inorganic hybrids, Inorg. Chem. 54 (2015) 2551–2559, https://doi.org/10.1021/ic502622k.

[8] M.H. Alizadeh, K.T. Holman, M. Mirzaei, H. Razavi, Triprolinium 12-hosphomolybdate: synthesis, crystal structure and properties of $[C_5H_{10}NO_2]_3[PMo_{12}O_{40}].4.5H_2O$, Polyhedron 25 (2006) 1567–1570, https://doi.org/10.1016/j.poly.2005.10.036.
[9] P. Wu, J. Zhang, X. Xu, J. Hao, Z. Xiao, C. Lv, F. Xiao, Either of left-right hands fits into an identical glove: a new crystal of polyoxometalate-amino acid salt, J. Clust. Sci. 21 (2010) 173–179, https://doi.org/10.1007/s10876-010-0303-0.
[10] H.-Y. An, E.-B. Wang, D.-R. Xiao, Y.-G. Li, Z.-M. Su, L. Xu, Chiral 3D architectures with helical channels constructed from polyoxometalate clusters and copper–amino acid complexes, Angew Chemie Int. Ed. 45 (2006) 904–908, https://doi.org/10.1002/anie.200503657.
[11] D. Liu, H.-Q. Tan, W.-L. Chen, Y.-G. Li, E.-B. Wang, Resolution of chiral polyoxoanion $[P_2Mo_{18}O_{62}]^{6-}$ with histidine, CrystEngComm 12 (2010) 2044, https://doi.org/10.1039/c001160f.
[12] Y. Wang, H. Li, C. Wu, Y. Yang, L. Shi, L. Wu, Chiral heteropoly blues and controllable switching of achiral polyoxometalate clusters, Angew. Chemie. Int. Ed. 52 (2013) 4577–4581, https://doi.org/10.1002/anie.201209497.
[13] Y. Zhao, L. Yin, J. Liu, H. Chen, W. Zhang, Helical screw sense bias in chiral polyfluorene stimulated by solvent, Chirality 29 (2017) 107–114, https://doi.org/10.1002/chir.22677.
[14] A. Pérez-Mellor, A. Zehnacker, Vibrational circular dichroism of a 2,5-diketopiperazine (DKP) peptide: evidence for dimer formation in cyclo LL or LD diphenylalanine in the solid state, Chirality 29 (2017) 89–96, https://doi.org/10.1002/chir.22674.
[15] A.J. Adler, N.J. Greenfield, G.D. Fasman, Circular Dichroism and Optical Rotatory Dispersion of Proteins and Polypeptides, 1973, pp. 675–735, https://doi.org/10.1016/S0076-6879(73)27030-1.
[16] H.D. Flack, Chiral and Achiral Crystal Structures, Helv. Chim. Acta, 86 (2003) 905–921, https://doi.org/10.1002/hlca.200390109.
[17] P.-P. Zhang, J. Peng, A.-X. Tian, J.-Q. Sha, H.-J. Pang, Y. Chen, M. Zhu, Y.-H. Wang, A series of compounds based on the Anderson-type polyoxoanions and Cu-amino acid complexes, J. Mol. Struct. 931 (2009) 50–54, https://doi.org/10.1016/j.molstruc.2009.05.020.
[18] M. Arefian, M. Mirzaei, H. Eshtiagh-Hosseini, A. Frontera, A survey of the different roles of polyoxometalates in their interaction with amino acids, peptides and proteins, Dalton Trans. 46 (2017) 6812–6829, https://doi.org/10.1039/C7DT00894E.
[19] G.A. Tsigdinos, Heteropoly molybdate anions of certain fifth group and, Ph.D. Thesis, Boston University, Boston, MA, 1961.
[20] H.C. Joo, K.M. Park, U. Lee, I.D. Brown, Crystal structure of the Anderson type hetero polyoxometalate; $K_2[H_7CrIIIMo_6O_{24}].8H_2O$: a redetermination revealing the position of the extra H atom in the polyanion, Acta Crystallogr. Sect. E Struct. Rep. Online 71 (2015) 157–160, https://doi.org/10.1107/S2056989015000390.
[21] K.-M. Park, H.-C. Joo, U. Lee, Crystal structure of potassium sodium heptahydrogen hexamolybdocobaltate(III) octahydrate: an extra-protonated B-series Anderson-type heteropolyoxidometalate, Acta Crystallogr. Sect. E Crystallogr. Commun 71 (2015) 1032–1035, https://doi.org/10.1107/S2056989015014784.
[22] C. Martin, C. Lamonier, M. Fournier, O. Mentré, V. Harlé, D. Guillaume, E. Payen, Preparation and characterization of 6-molybdocobaltate and 6-molybdoaluminate cobalt salts. Evidence of a new heteropolymolybdate structure, Inorg. Chem. 43 (2004) 4636–4644, https://doi.org/10.1021/ic0354365.
[23] V. Reyes-Márquez, K.O. Lara, M. Sánchez, J.C. Gálvez-Ruiz, Unconventional hydrogen and dihydrogen bonded supramolecular array of a 2,6-dioxa-9,16-diaza-1,3(1,2),4(1,4)-tribenzenacycloheptadecaphane-borane adduct, Arkivoc 2008 (2008) 115–123.
[24] E. Cauët, M. Rooman, R. Wintjens, J. Liévin, C. Biot, Histidine–Aromatic interactions in proteins and Protein–Ligand complexes: quantum chemical study of x-ray and model structures, J. Chem. Theory Comput. 1 (2005) 472–483, https://doi.org/10.1021/ct049875k.
[25] N. Gao, H. Sun, K. Dong, J. Ren, T. Duan, C. Xu, X. Qu, Transition metal-substituted polyoxometalate derivatives as functional anti-amyloid agents for Alzheimer's disease, Nat. Commun. 5 (2014) 3422–3430, https://doi.org/10.1038/ncomms4422.
[26] H. Aghabozorg, H. Eshtiagh-Hosseini, a. R. Salimi, M. Mirzaei, A brief review on formation of $(H_2O)_n$ clusters in supramolecular proton transfer compounds and their complexes, J. Iran. Chem. Soc. 7 (2010) 289–300, https://doi.org/10.1007/BF03246013.
[27] I. Rozas, I. Alkorta, J. Elguero, Bifurcated hydrogen bonds: three-centered interactions, J. Phys. Chem. A 102 (1998) 9925–9932, https://doi.org/10.1021/jp9824813.
[28] O. Markovitch, N. Agmon, The distribution of acceptor and donor hydrogen-bonds in bulk liquid water, Mol. Phys. 106 (2008) 485–495, https://doi.org/10.1080/00268970701877921.
[29] R. Parthasarathy, Crystal structure of glycylglycine hydrochloride, Acta Crystallogr. Sect. B 25 (1969) 509–518, https://doi.org/10.1107/s0567740869002482.
[30] D. June Sutor, The C–H··· O hydrogen bond in crystals, Nature 195 (1962) 68–69, https://doi.org/10.1038/195068a0.
[31] C.I. Cabello, F.M. Cabrerizo, A. Alvarez, H.J. Thomas, Decamolybdodicobaltate(III) heteropolyanion: structural, spectroscopical, thermal and hydrotreating catalytic properties, J. Mol. Catal. A Chem. 186 (2002) 89–100, https://doi.org/10.1016/S1381-1169(02)00043-2.
[32] J.F. Pearson, M.A. Slifkin, The infrared spectra of amino acids and dipeptides, Spectrochim. Acta Part A Mol. Spectrosc. 28 (1972) 2403–2417, https://doi.org/10.1016/0584-8539(72)80220-4.